analytical chemistry

Article

pubs.acs.org/ac

# Broadly Available Imaging Devices Enable High-Quality Low-Cost Photometry

Dionysios C. Christodouleas,[†] Alex Nemiroski,[†] Ashok A. Kumar,[†] and George M. Whitesides*[,†,‡,§]

[†]Department of Chemistry & Chemical Biology, Harvard University, 12 Oxford Street, Cambridge, Massachusetts 02138, United States

[‡]Wyss Institute for Biologically Inspired Engineering, Harvard University, 60 Oxford Street, Cambridge, Massachusetts 02138, United States

[§]Kavli Institute for Bionano Science & Technology, Harvard University, 29 Oxford Street, Cambridge, Massachusetts 02138, United States

Supporting Information

**ABSTRACT:** This paper demonstrates that, for applications in resource-limited environments, expensive microplate spectrophotometers that are used in many central laboratories for parallel measurement of absorbance of samples can be replaced by photometers based on inexpensive and ubiquitous, consumer electronic devices (e.g., scanners and cell-phone cameras). Two devices, (i) a flatbed scanner operating in transmittance mode and (ii) a camera-based photometer (constructed from a cell phone camera, a planar light source, and a cardboard box), demonstrate the concept. These devices illuminate samples in microtiter plates from one side and use the RGB-based imaging sensors of the scanner/camera to measure the light transmitted to the other side. The broadband absorbance of samples (RGB-resolved absorbance) can be calculated using the RGB color values of only three pixels per microwell. Rigorous theoretical analysis establishes a well-defined relationship between the absorbance spectrum of a sample and its corresponding RGB-resolved absorbance. The linearity and precision of measurements performed with these low-cost photometers on different dyes, which absorb across the range of the visible spectrum, and chromogenic products of assays (e.g., enzymatic, ELISA) demonstrate that these low-cost photometers can be used reliably in a broad range of chemical and biochemical analyses. The ability to perform accurate measurements of absorbance on liquid samples, in parallel and at low cost, would enable testing, typically reserved for well-equipped clinics and laboratories, to be performed in circumstances where resources and expertise are limited.

Absorbance spectroscopy is the most common analytical technique used for chemical and biochemical analyses. Solution-based test kits (e.g., tube test kits and microtiter plate ELISA kits) are commercially available for hundreds of important analytes (e.g., metabolites, proteins, environmental pollutants), can provide accurate and precise results, and are inexpensive (the cost-per-sample of these test kits is typically < $5). Although these characteristics make absorbance spectroscopy attractive for use in laboratories and clinics across the world, the required instrumentation (e.g., spectrophotometers and microplate spectrophotometers) can cost from $2 000 to $50 000, depending on their specifications, versatility, and throughput. Laboratories and clinics in low- and middle-income countries typically (i) cannot afford this expensive instrumentation; (ii) do not have access to the components, personnel, and expertise required to maintain the equipment; and/or (iii) lack the infrastructure (e.g., continuous and stable electrical power) necessary to keep it running.[1] A simple, low-cost alternative to conventional spectrophotometric equipment would greatly reduce the barriers to providing modern medical and environmental testing to low- and middle-income countries.

Here, we report the adaptive use of ubiquitous consumer electronic devices to perform low-cost photometry suitable for use in resource-limited environments. We demonstrate that (i) a commercially available *flatbed scanner* with a transmittance mode for imaging photographic films and (ii) a portable, *camera-based photometer*—constructed from a paper box that houses a white, LED-based, planar light source for sample illumination, and a cell-phone camera (which is provided by the user) as a detector—can be used to perform sensitive absorbance measurements on multiple liquid samples stored in a microtiter well plate, in parallel, with accuracy and precision comparable to microplate spectrophotometers.

Previously, we and others have demonstrated adaptive use of digital cameras and flatbed scanners as low-cost detectors for

**Received:** April 7, 2015
**Accepted:** August 4, 2015
**Published:** August 4, 2015





DOI: 10.1021/acs.analchem.5b01612
*Anal. Chem.* 2015, 87, 9170−9178

colorimetric assays performed on test strips (e.g., dipstick tests, immunochromatographic lateral flow tests) and paper devices.[2−16] Ozcan and co-workers and Henry and co-workers have recently reviewed the literature in the field.[17−19] Test strips, however, typically only provide semiquantitative results; for full quantitation, test kits for liquid samples remain the gold standard.

To develop low-cost photometers for measuring the absorbance of liquid samples, other efforts have typically used colored, light-emitting diodes (LEDs) to illuminate a liquid sample from one side and a photodetector (photoresistor, phototransistor, or photodiode) on the other side to detect the light transmitted through the sample.[20−29] For example, we and others have constructed low-cost photometers based on this principle to measure (i) antibodies against HIV in serum,[21] (ii) hemoglobin[22,23] in blood, and (iii) fluoride[27] and mercury[29] in water samples. Although low-cost photometers based on this approach have filled important needs in specific analytical applications (e.g., for measuring hemoglobin[22]), they have two important limitations: (i) they are not sufficiently versatile to perform measurements at multiple wavelengths; that is, they can only perform measurements at the specific wavelengths defined by the LED used, and (ii) they are incapable of high-throughput measurements using microtiter plates (which typically have 96 wells).

To address the limitations of systems that use narrowband LEDs for illumination, others have performed optical measurements of liquid samples using broadband light emitted by flatbed scanners[30,31] or digital displays (e.g., computer monitors,[32−36] tablet computers,[37] and digital photo displays[26]) and used the image sensors found in flatbed scanners,[30,31] Web cameras,[32−36] or smartphone cameras[37] as detectors. For example, De Lelis et al. and Abbaspour et al. used reflectance-based flatbed scanners to image test solutions and then correlated the measured color of the test solution with the concentration of a chromogenic compound.[30,31] The reflectance-based approach, however, is problematic because the variability of the color values across the sample, due to variability and complexity of the optical path length of reflected light, greatly complicates the calculation of absorbance and the precision of measurements. An alternative approach uses the light transmitted through the sample to measure absorbance. Fillipini and co-workers were the first to use consumer electronic devices to measure the transmittance of liquid samples.[32] They used computer monitors (i.e., cathode ray tube (CRT) or liquid crystal display (LCD)) to display a controlled sequence of colors that illuminates the sample from one side, while a Web camera recorded the transmitted light from the opposite side. A Matlab-based program decomposed the video file into individual frames and calculated the gray scale value of the transmitted light.

This approach, and other similar approaches that have used consumer electronic devices,[30−37] have two important drawbacks: (i) they require custom software to extract the intensity of the light from the image of a sample and (ii) they require digital displays, which are expensive, and, in some cases, not portable (e.g., monitors), as light sources. Furthermore, although transmittance should, in principle, yield more precise and better-understood results than reflectance, previous efforts have not established a clear and well-defined relationship between the analytical signal and absorbance spectrum. This paper has three objectives: (i) to demonstrate the applicability of inexpensive photometers based on broadly available consumer electronic devices (i.e., flatbed scanners and cell-phone cameras) to perform high-quality, high-throughput measurement of absorbance of samples, (ii) to establish a well-defined relationship between the absorbance of light (as measured by these commercial image sensors) and the absorbance spectra of samples (as measured by a laboratory spectrophotometer), (iii) to outline the conditions required for performing high-quality, high-throughput measurement of absorbance using photometers that use RGB-based CCD/CMOS image sensors; these conditions can be used by academic laboratories and companies to design low-cost photometers for chemical and biochemical analysis.

In this work, we used two low-cost photometers, a *flatbed scanner* and a *camera-based photometer*, that employ white, broadband LEDs as light sources and CCD/CMOS image sensors as photodetectors. By placing a microtiter plate (containing the samples) between the light source and the photodetector, we captured the images of the samples. In this configuration, the light source illuminates the sample with visible light (∼400−700 nm) from one side, and the pixel sensors of the imaging sensor digitize the intensity of the light, transmitted to the other side, into three color channels: red (R), green (G), and blue (B). An image of a microtiter plate contains images of several samples that can be analyzed separately, and therefore, multiple liquid samples can be analyzed, in parallel. By using the color values of a sample, we calculated the broadband "RGB-resolved absorbance" of the sample. We compared the "RGB-resolved absorbance" of solutions of 11 dyes to the peak absorbance measured using a microplate spectrophotometer, and we established a rigorous relationship between the "RGB-resolved absorbance" of a sample and the measured absorbance spectrum of an analyte. We demonstrated that the *flatbed scanner* and the *camera-based photometer* could replace microplate spectrophotometers in a broad range of biochemical and environmental assays and enable high-quality photometric assays to be performed in low-resource and remote settings.

## EXPERIMENTAL SECTION

**Materials and Chemicals.** We purchased a *flatbed scanner* (Epson Perfection V500 photo, Epson) for $90 from www.amazon.com and a low-cost, planar light source (edge-lit LED backlight for iPhone 5) for $6 from www.Tmart.com. We also used a cell-phone camera (OPTIMUS F3 4G LTE, LG). Absorbance measurements were performed using a *microplate spectrophotometer* (SpectraMax M2, Molecular Devices). All chemicals and reagents were used as received without further purification (see the Supporting Information for the suppliers). We used ImageJ or Microsoft Paint to read the color intensity (RGB values) of a pixel of an image.

**Configuration of the Devices.** The *flatbed scanner* employs a CCD image sensor in a strip and operates in two different modes: reflectance and transmittance. The transmittance mode is designed for imaging photographic films and uses a built-in transparency unit that employs a planar light source in a strip (Figure 1A). Both the light source of the transparency unit and the image sensor scan across the imaging surface of the scanner simultaneously to capture an image. We placed a 96-well microtiter plate containing samples into the *flatbed scanner* (that is, between the imaging surface of the scanner and the transparency unit) (Figure 1A). Although an ∼1 cm gap persisted after closing the lid of the scanner, the gap was small enough that the external light did not influence the


DOI: 10.1021/acs.analchem.5b01612
*Anal. Chem.* 2015, 87, 9170−9178

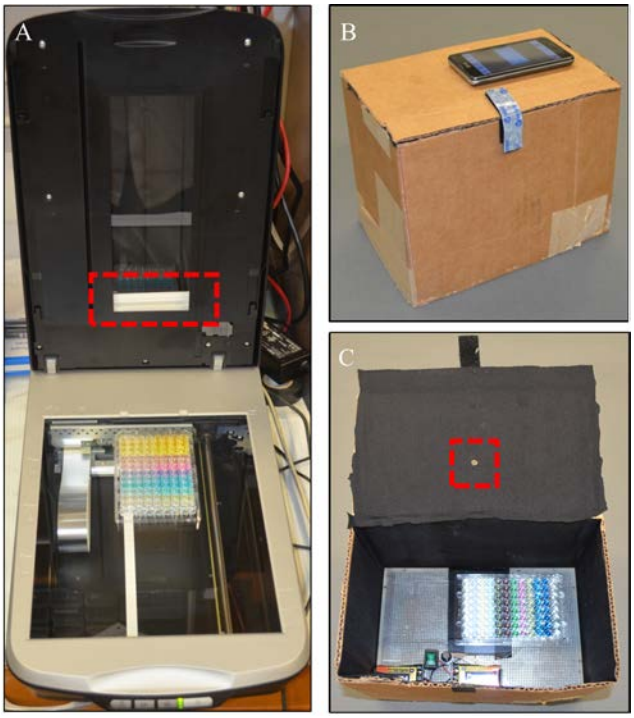


**Figure 1.** Images of (A) the *flatbed scanner* ready to scan a microtiter plate (the planar light source is outlined by the red, dashed line); (B) the *camera-based photometer*; (c) the microtiter plate inside the *camera-based photometer* with the planar light source activated (the small aperture in the lid of the box is outlined by the red, dashed line).

imaging of the microtiter plate. The imaging area of the *flatbed scanner* in transmittance mode (27 cm × 8.3 cm) is large enough to image up to two standard microtiter plates in parallel. Using the software bundled with the scanner, we disabled all automatic correction functions to ensure that the photometric data were not manipulated and then performed all scans in the transmittance mode (see Figure S-1 in the Supporting Information). We saved all images as Joint Photographic Experts Group (JPEG) files.

The *camera-based photometer* (Figure 1B and Figure S-2 in the Supporting Information) consisted of (i) a planar light source (edge-lit, LED backlight module found in most smartphones and tablet computers) to illuminate samples from below; (ii) a foldable cardboard box to prevent stray light from entering the detection region and to define a fixed imaging distance; and (iii) a cell phone with a CMOS camera (LG OPTIMUS F3 4G LTE) to photograph samples through a 6 mm hole in the lid of the box (see Supporting Information for details). Figure 2B shows how we arranged a microtiter plate (with samples) above the planar light source, which was large enough to illuminate 32 wells of a standard 96-microtiter plate. In this arrangement, three separate photos were acquired to image the entire plate (see Figure S-3A–C in the Supporting Information). When not in use, the box can be folded (see Figure S-3D in the Supporting Information) and the whole device can be stored in a backpack.

**Characterization of the CCD/CMOS Image Sensors and the White LEDs.** For each of the channels $k = \{R,G,B\}$, we characterized the spectral sensitivity $S_k(\lambda)$ of the CMOS/CCD image sensors (these data are not provided by the manufacturers of these devices and vary between different imaging devices) by using a broadband source of white light

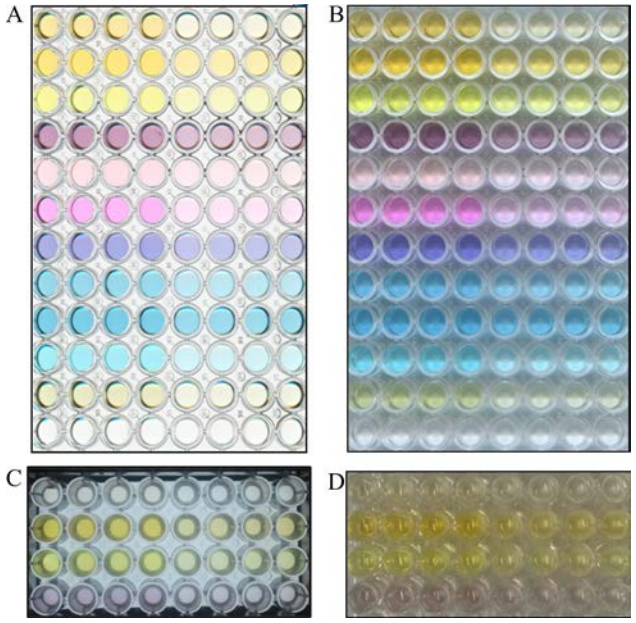


**Figure 2.** Images of a microtiter plate, containing solutions of 11 dyes (one per row) at two concentrations each (four left columns vs four right columns) and water (the twelfth row) imaged by the *flatbed scanner* in transmittance mode (A), the *flatbed scanner* in reflectance mode (B), the *camera-based photometer* (C), and the cell-phone camera in ambient light (D).

(Halogen Fiber Optic Lightsource, Cuda), a monochromator (SpectraPro-300i, Acton Research Corporation), and a fiber-optic spectrophotometer (HR4000+, Ocean Optics). We also used the spectrophotometer to characterize the spectra $L(\lambda)$ of light emitted by the sources of white light employed in both photometers.

**Comparison between Transmittance and Reflectance Measurements.** To demonstrate the superior quality of transmittance-based vs reflectance-based measurements of absorbance, we imaged standard solutions of 11 dyes (see the Supporting Information for concentrations) and water using (i) the *flatbed scanner* in transmittance mode (Figure 2A), (ii) the *flatbed scanner* in reflectance mode (Figure 2B), (iii) a flatbed scanner employing CIS technology (Canoscan, LIDE 60, Canon; see Figure S-4 in the Supporting Information), (iv) the *camera-based photometer* (Figure 2C), and (v) a cell-phone camera (see Figure 2D), which relies on ambient light (i.e., no planar light source or box). We read the color intensity (RGB values) of all the pixels in each well and estimated the distribution of the RGB values of the pixels in each well.

**Absorbance Measurements of Chromogenic Compounds.** We prepared solutions of 11 chromogenic compounds (disperse orange 3, methyl orange, fluorescein, 2,2-diphenyl-1-picrylhydrazyl (DPPH), eosin Y, rhodamine B, trypan blue, prussian blue, malachite green, methylene blue, chlorophyll b) at different concentrations (detailed in the Supporting Information) and measured the absorption spectra $A(\lambda)$ and peak absorbance $A_{peak}$ of these solutions using the *microplate spectrophotometer*. Importantly, these compounds exhibit absorbance peaks with very different spectral characteristics (e.g., shape, position, and intensity of the spectral peak) that span the entire visible spectrum (see Figure S-5 in the Supporting Information). We also captured the images of the microtiter plates that contain these solutions using the *flatbed scanner* and the *camera-based photometer*. We next read the RGB


DOI: 10.1021/acs.analchem.5b01612
*Anal. Chem.* 2015, 87, 9170–9178

values of three pixels, chosen at random from within the image of each solution, with ImageJ or Microsoft Paint (see Figures S-6 and S-7 in the Supporting Information) and recorded the mean values $C_k$ of each group of RGB values. Depending on the position of the peak absorbance of a compound, one color value of an RGB triplet typically provided more sensitive results than the other two. In the Supporting Information (see Figure S-8), we show that the blue color value is more suitable for absorbance peaks between 400 and 505 nm, the green color value is more suitable for peaks between 505 and 580 nm, and the red value for absorbance peaks between 580 and 700 nm. We used the above guidelines for the selection of the most appropriate color value (R, G, or B) to be used for the estimation of the RGB-resolved absorbance values of each solution.

**Applications in Biochemical and Environmental Analyses.** To demonstrate the use of the *flatbed scanner* and the *camera-based photometer* in laboratory and clinical applications, we compared the performance of these devices vs a *microplate spectrophotometer* in six photometric assays for the determination of (i) lactic acid in human serum using an enzymatic assay; (ii) low-density lipoproteins (LDL) in human serum using a competitive ELISA; (iii) anti-*Treponema pallidum* antibodies in human serum using an indirect ELISA; (iv) total protein in solutions of antibodies using the Bicinchoninic acid (BCA) assay; (v) hemoglobin in whole blood using the Cyanomethemoglobin assay; and (vi) nitrite ions in samples of water using the Griess assay (see Supporting Information for details). For all assays, we used commercially available test kits or ready-to-use reagents (see the experimental details in the Supporting Information). Figure S-9 in the Supporting Information shows the absorbance spectra of the products of each assay.

## RESULTS AND DISCUSSION

**Comparison between Transmittance and Reflectance Measurements.** Previous approaches to low-cost optical analysis of samples in microtiter plates have used flatbed scanners in reflectance mode.[32,33] Using reflected light to estimate absorbance, however, is problematic because the path that reflected light takes through each sample is complex. Depending on the geometry and divergence angle of the light source, the many different air/liquid/plastic interfaces present around the sample scatter the light at multiple locations and in different ways. This scattering cause the colors (RGB values) of the image to be nonuniform across each well.[32] This variation in the pixel values originates from the angled configuration of the light source and the photodetector used by the scanner when imaging in reflectance mode.[18] In an attempt to compensate for these artifacts, approaches based on reflectance-mode imaging use custom software to spatially average the RGB values of all pixels within each well, and then to calibrate the relationship between the average RGB values and the concentration of the analyte.[32,33] Establishing a well-understood relationship between these mean values and the concentration of the analyte, however, remains complicated for two reasons: (i) the definition of "mean" value is ambiguous because there is typically a multimodal distribution of the RGB color values across each well and (ii) the complex and highly variable optical path-length precludes the establishment of a well-defined analytical relationship between the intensity of light that reaches the detector and the concentration of the analyte.

A better, simpler approach to perform low-cost, high-quality absorbance measurements is to detect the light transmitted through a sample. In this case, the alignment between the light source and the detector establishes an optical path length that is simple, well-defined, and spatially uniform across the plate.

Figure 3 show examples of the distribution of the values of the green color channel for pixels within a single well

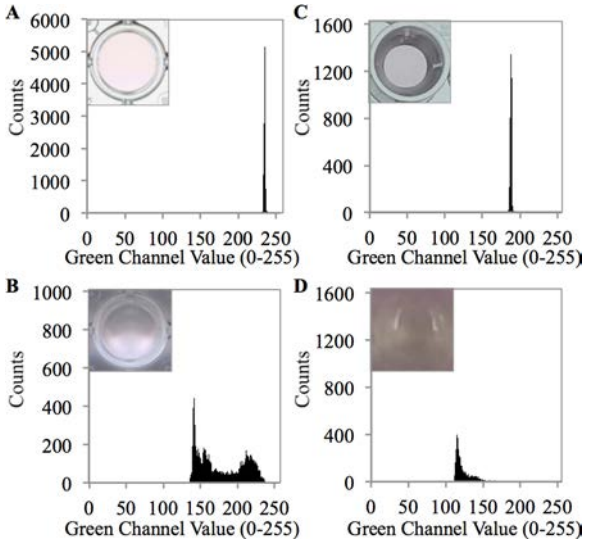


**Figure 3.** Histograms of the green channel values throughout an image of a well (inset) containing a 6.00 $\mu$M Eosin Y solution captured using the *flatbed scanner* in transmittance mode (A) and reflectance mode (B), the *camera-based photometer* (C) and the cell-phone camera in ambient light (D).

containing a solution of eosin Y captured using the *flatbed scanner* in transmittance mode and in reflectance mode, a scanner (using CSI technology) in reflectance mode, the *camera-based photometer*, and a cell-phone camera relying on ambient light. For measurements taken using the *flatbed scanner* in transmittance mode (Figure 3A), the mean and mode of the pixel values differed by only 0.4%, and the % RSD of the pixel values in each well was 0.4% ($N$ = 10 024) (see Figure S-10 in the Supporting Information). In the case of the measurements taken using the *camera-based photometer* (Figure 3C), the mean and mode of the pixel values differed by only 0.05%, and the % RSD of the pixel values in each well was 0.6% ($N$ = 3532) (see Figure S-11 in the Supporting Information). These low values indicate that the value of each pixel is nearly identical across the well, for both transmittance-based measurements. Using Hartigan's Dip test of unimodality,[38] we verified that the distribution of pixel values was unimodal in both cases (see Figures S-10 and S-11 in the Supporting Information). By contrast, for reflectance measurements, the distribution of the color values of the pixels in each well was broad. For example, for measurements taken using the scanner in reflectance mode (Figure 3B), the mean and mode of the pixel values differed by 21% (see Figure S-10 in the Supporting Information). For measurements taken using the cell-phone camera without the box and the planar light source (Figure 3D), the mean and mode of the pixel values differed by 8% (see Figure S-11 in the Supporting Information). Using Hartigan's Dip test of unimodality,[38] we verified that the distribution of pixel values was not unimodal for either of the reflectance-based measurements (see Figures S-10 and S-11in the Supporting


DOI: 10.1021/acs.analchem.5b01612
*Anal. Chem.* 2015, 87, 9170−9178

Information). We found that these statistics were consistent for all wells and for all 11 chromogenic compounds. For a distribution that is not unimodal, a randomly chosen pixel in the well will not correlate well to the mean of the population. For a broad distribution, a randomly chosen pixel will be unlikely to be close to the mean of the population. To average out these variations and provide reproducible results, in reflectance-based measurements, custom image processing and analysis are necessary to estimate the mean of the population.

The narrow distribution of the color values of the pixels for transmittance-based measurements enables a precise estimation of the mean value by sampling only a few pixels. Using eq 1, which assumes that the distribution of color values follow a normal distribution in each well, we estimated the number of pixels $N$ necessary to read to achieve a sample mean (the average of the color values of $N$ pixels) that does not deviate from the population mean (the average of the color values of all pixels) by more than $\varepsilon$ (the percentage of difference between sample mean and population mean), within a confidence level determined by the value of $z$ (which can be found in a standard tables for statistical analysis[39]), and given the relative standard deviation RSD of the population.

$$N = \left(\frac{z}{\varepsilon}\mathrm{RSD}\right)^2 \tag{1}$$

For transmittance measurements using the *flatbed scanner* and the *camera-based photometer*, the RSD value of color values of all pixels within each well is less than 0.006. With this RSD, achieving a sample mean that is within 1% of the population mean ($\varepsilon$ = 0.01), with 95% confidence ($z$ = 1.96), requires sampling $N$ = 1.38 (~2) pixels. This characteristic vastly reduces the image processing necessary to measure transmittance, simplifies the procedure, and makes it feasible without any specialized software. To eliminate erroneous results due to the sampling of an outlier, we decided to average the RGB values of three pixels from the image of each well. We selected three pixels at random (by manually choosing random places inside the image of a well), read their RGB color values $C_k$ with ImageJ or Microsoft Paint, and averaged these values together, for each color channel.

**Definition and Origin of RGB-Resolved Absorbance.** Unlike peak absorbance $A_{peak}$ measured by traditional spectrophotometers that detect light at a specific wavelength, RGB-resolved absorbance, $A_k$, could be measured using RGB-based photometers. These photometers are based on imaging devices (e.g., scanners, cell phone cameras) and detect light over a broad bandwidth. One of the central goals of this paper is to define the relationship between the broadband absorbance, calculated using RGB color values, and the absorbance spectrum of a sample $A(\lambda)$. To quantify broadband absorption and define its relationship to $A(\lambda)$, we need to understand how an image sensor converts the spectral intensity of captured light $I(\lambda)$ into RGB values.

Digital imaging devices use image sensors, which consist of an array of pixel sensors, to convert light intensity to electrical current.[40,41] Each individual pixel sensor employs a CCD or CMOS photodetector with a spectral responsivity $R(\lambda)$ (conversion of photons to electrons), and red, green, and blue color filters, each with transmittance $F_k(\lambda)$, where $k = \{R, G, B\}$. The total spectral sensitivity of each pixel sensor is $S_k(\lambda) = R(\lambda)F_k(\lambda)$. Every pixel of an image, captured by a digital imaging device, has a set of raw, measured values $\zeta_k$ that are correlated with the spectral intensity $I(\lambda)$ by $\zeta_k = \int_{\lambda_1}^{\lambda_2} I(\lambda) S_k(\lambda)\mathrm{d}\lambda$, where $(\lambda_1, \lambda_2)$ define the range of wavelengths over which the sensor can detect light.[42]

To reproduce colors better (e.g., more as they appear in real life), digital imaging sensors typically impose a nonlinear "gamma" correction before each color value $C_k$ is recorded, according to the relation, $C_k = \beta_k(\zeta_k)^{\gamma_k}$, where $\beta_k$ is a linear correction factor and $\gamma_k$ is an exponential correction factor, which can be different for each color channel.[41] The value of each color channel encoded into the captured image is therefore described by $C_k = \beta_k(\int_{\lambda_1}^{\lambda_2} I(\lambda)S_k(\lambda)\mathrm{d}\lambda)^{\gamma_k}$. For a sample with absorbance spectrum $A(\lambda)$ and for a light source with spectrum $L(\lambda)$, the intensity of the spectral intensity reaching the detector is $I(\lambda) = L(\lambda)10^{-A(\lambda)}$. The set of the recorded RGB values of each pixel of the image of the sample is therefore given by eq 2.

$$C_k = \beta_k\left[\int_{\lambda_1}^{\lambda_2} L(\lambda)10^{-A(\lambda)}S_k(\lambda)\mathrm{d}\lambda\right]^{\gamma_k} \tag{2}$$

Using the equation for estimating peak absorbance ($A_{peak} = -\log_{10}(I_S/I_B)$, see Supporting Information for a detailed definition), we define the RGB-resolved absorbance $A_k$ of a sample (with measured color value $C_k^{(S)}$) to a blank solution (with measured color value $C_k^{(B)}$) by eq 3.

$$A_k \equiv -\log_{10}\left[\frac{C_k^{(S)}}{C_k^{(B)}}\right] \tag{3}$$

Substitution of eq 2 into eq 3 yields eq 4, which relates $A_k$ to $A_S(\lambda)$ and $A_B(\lambda)$.

$$A_k = -\gamma_k \log_{10}\left[\frac{\int_{\lambda_1}^{\lambda_2} L(\lambda)10^{-A_S(\lambda)}S_k(\lambda)\mathrm{d}\lambda}{\int_{\lambda_1}^{\lambda_2} L(\lambda)10^{-A_B(\lambda)}S_k(\lambda)\mathrm{d}\lambda}\right] \tag{4}$$

It is important to note that this general of absorbance applies not only to broadband RGB-based photometers, but also to all types of photometers (see the Supporting Information for details).

Through extensive characterization, we estimated $S_k(\lambda)$ and $\gamma_k$ for all the color channels of the image sensors of the *flatbed scanner* and the *camera-based photometer* (see the Supporting Information for details). Using eq 4 and (i) the $L(\lambda)$ of the transparency unit of the *flatbed scanner* and the planar light source of the *camera-based photometer*, (ii) the $A(\lambda)$ of 11 different dyes measured at a range of concentrations by the *microplate spectrophotometer*, and (iii) the extracted values of $S_k(\lambda)$ and $\gamma_k$, we estimated the expected $A_k$ for all the standard compounds. We also calculated the measured $A_k$ for all the dyes and we compared them to the expected $A_k$. Figure S-12 in the Supporting Information shows plots that demonstrate the strong correlation between the expected and measured values of $A_k$. As an example, Figure S-8 in the Supporting Information outlines the steps used to estimate $A_k$ for a 10 $\mu$M solution of methylene blue for the *flatbed scanner* and the *camera-based photometer*.

**Comparison of RGB-Resolved Absorbance with Peak Absorbance.** We compared the values of peak absorbance $A_{peak}$ (measured by the microplate spectrophotometer) with RGB-resolved absorbance $A_k$ (measured by the low-cost photometers) of solutions of different concentration of all 11



DOI: 10.1021/acs.analchem.5b01612
*Anal. Chem.* 2015, 87, 9170−9178

chromogenic compounds. Figure S-13 in Supporting Information shows three examples of the correlation lines of $A_{peak}$ *vs* $A_k$; Table S-1 of the Supporting Information lists the analytical characteristics of all the correlation lines. For all cases, we determined a positive, near-unity correlation between the $A_k$ and $A_{peak}$ (correlation coefficient $r > 0.99$). Because the value of $A_{peak}$ is always, by definition, greater than the value of $A_k$, all slopes of the correlation lines were always greater than unity. Equation 4 shows that this behavior occurs for two important reasons: the polychromatic nature of RGB-resolved absorbance and the gamma correction. Relative to a standard narrowband measurement at $\lambda_{peak}$, broadening the optical bandwidth of the measurement and/or misaligning $\lambda_{peak}$ with respect to the peak value of $L(\lambda)S_k(\lambda)$ can only serve to decrease the sensitivity to changes in concentration. This effect occurs because $\int_{\lambda_1}^{\lambda_2} L(\lambda)10^{-A(\lambda)}S_k(\lambda)d\lambda)$ necessarily includes regions where $A(\lambda) < A_{peak}$. In this case, the light that does not interact much (or at all) with the analyte will contribute more to the raw RGB color values $\zeta_\kappa$ than light transmitted near $\lambda_{peak}$; in this case, the ratio between the raw RGB values, captured from the light transmitted through the sample relative to the blank, will tend to unity ($\zeta_k^{(S)}/\zeta_k^{(B)} \rightarrow 1^-$), and therefore, $A_k < A_{peak}$ for any absorbance spectrum $A(\lambda)$. For example, solutions of rhodamine B and eosin Y that exhibit similar values of $A_{peak}$ as well as overall spectral shape $A(\lambda)$ (shown in Figure S-5 in the Supporting Information) may still exhibit very different values of green-resolved absorbance $A_G$ (~3−4× difference) because, compared to eosin Y, the position of $\lambda_{peak}$ of rhodamine B is better-aligned with the peak of $L(\lambda)S_G(\lambda)$.

The nonlinear gamma correction that all imaging equipment imposes also serves to distort the magnitude of $A_k$. In particular, because $\gamma_k < 1$ for all the devices that we characterized, the gamma corrections always tended to further reduce $A_k$ compared to a narrowband measurement centered at $\lambda_{peak}$. Although the gamma correction reduces the sensitivity to changes in concentration, it does not change the linearity of the $A_k$, and therefore, any image sensor can be calibrated easily for linear measurements of absorbance without knowing the values of the gamma correction factors.

**Absorbance Measurements of Chromogenic Compounds.** We used the RGB-resolved absorbance $A_k$ of solutions of each chromophore measured with the low-cost photometers (i.e., the *flatbed scanner* in transmittance mode and the *camera-based photometer*) and the peak absorbance $A_{peak}$ of the same solutions of chromophores measured with the *microplate spectrophotometer*, to calculate the calibration lines for $A_k$ and $A_{peak}$ vs the concentration of all 11 chromophores, for each photometer. As an example, Figure 4 shows the calibration curves of DPPH vs concentration; Table S-2 in the Supporting Information reports the remaining calibration curves. In all cases, the curves were linear, and the limits-of-detection of concentration of the dyes, measured by both the *microplate spectrophotometer* and the low-cost photometers, were comparable.

These results demonstrate that RGB-based photometers, such as the ones we demonstrated, can be useful for absorbance measurements, regardless of the shape, position, or intensity of the peak absorbance $A_{peak}$ of the sample. The ultimate sensitivity of the measurements to changes in concentration of the sample, however, will depend strongly on the position and the shape of $A_{peak}$ relative to the spectral peaks of $L(\lambda)S_k(\lambda)$ for a chosen source of illumination and imaging sensor. The

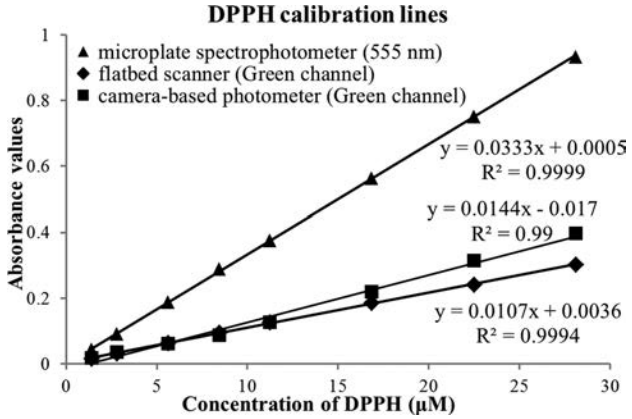


**Figure 4.** Calibration curves of the absorbance values (either $A_{peak}$ for the microplate spectrophotometer or $A_k$ for the *flatbed scanner* and *camera-based photometer*) vs the concentration of DPPH. Each data point corresponds to the mean value of seven measurements; the standard deviations are smaller than the symbols used for each point.

better the alignment of $A_{peak}$, for a chosen sample, with the peaks of $L(\lambda)S(\lambda)$, for each color channel, the more sensitive the measurements will be. Importantly, despite the reduced sensitivity of the different RGB-based measurements relative to those performed with a *microplate spectrophotometer*, we do not observe a corresponding decrease in precision or limit-of-detection. We conclude, therefore, that the sensitivity of RGB-based measurements will not limit the applicability of RGB-based photometers. In the case that increased sensitivity is desired, however, there are two strategies to achieve it. (i) When developing an assay, choosing or engineering dyes with narrow peaks that are centered on the peaks of $L(\lambda)S(\lambda)$ will ensure maximal sensitivity to differences in concentration. (ii) Addition of bandpass color filters centered on the absorption peaks of the samples would further improve sensitivity by transmitting the light that interacts most strongly with the sample and blocking intense background light that depends only weakly on the concentration of the analyte.

RGB-based photometers can, in principle, also enable quantification and discrimination between unknown concentrations of colored compounds in a mixture if, and only if, they satisfy the following three criteria: (i) the three values of $A_k$ for each constituent compound are known (for example, at a standard, known concentration); (ii) there are no more than three different compounds in the mixture (this condition arises because there are only three degrees of freedom in each measurement: $A_R$, $A_G$, and $A_B$); (iii) the values of $A_k$ of the different compounds are linearly independent, that is, the column vectors $A^{(n)} = \{A_R^{(n)}; A_G^{(n)}; A_B^{(n)}\}$ of RGB-resolved absorbances of each compound, indexed $n = \{1, 2, 3\}$ must satisfy $\det[\{A^{(1)}, A^{(2)}, A^{(3)}\}] = 0$. If all three criteria are satisfied, then a single photometric measurement can be used to estimate the concentrations of each of the three compounds. In cases where the $A_k$ are not linearly independent, as may be the case if some or all of the absorption peaks occur within the same color channel, or if discrimination between more than three compounds is desired, it may be possible to satisfy these condition by adding extra degrees of freedom, for example, by comparing multiple measurements with and without bandpass color filters.

**Applications in Biochemical and Environmental Analyses.** We compared the performance of the *flatbed*


DOI: 10.1021/acs.analchem.5b01612
*Anal. Chem.* 2015, 87, 9170−9178

*scanner* and *camera-based photometer* against a *microplate spectrophotometer* (used as the laboratory standard) as detectors in six important assays for the determination of (i) lactic acid in human serum; (ii) low-density lipoproteins (LDL) in human serum; (iii) anti-*Treponema pallidum* antibodies in human serum; (iv) total protein in solutions of antibodies; (v) hemoglobin in whole blood; and (vi) nitrite ions in samples of water. We chose these assays because (i) they are commonly used in biochemical or environmental analyses and (ii) they are representative of common chemical assays (e.g., enzymatic assay, immunoassay, and chromogenic assay). The Lactate assay is used to measure the concentration of lactic acid in serum and is representative of other assays to detect common serum components (e.g., glucose, creatinine, alkaline phosphatase). The LDL ELISA is used to measure the concentration of low-density lipoproteins in serum and is representative of other immunoassays of common biomarkers (e.g., carcinoembryonic antigen, troponin). The anti-*Treponema pallidum* IgG ELISA is used to detect syphilis and is representative of other qualitative ELISA tests to detect infectious diseases (e.g., dengue fever, Ebola, malaria). The Cyanmethemoglobin assay is the gold-standard method to detect hemoglobin in blood. The Bicinchoninic acid (BCA) assay is the gold-standard method to measure the total protein concentration of purified biological samples. The Griess assay is used to measure the concentration of nitrite ions in water samples and is representative of other simple chromogenic assays for the detection of pollutants in environmental samples (e.g., chlorine, metal ions).

Figure 5 and Table S-3 of the Supporting Information compares the results of analyses of real samples measured with the *flatbed scanner*, the *camera-based photometer* and the *microplate spectrophotometer*. Using a *t* test, we found that the results we obtained using the *flatbed scanner* and the *camera-based photometer* were not significantly different than those obtained with the *microplate spectrophotometer*. From these data, we conclude that these low-cost photometers can replace a *microplate spectrophotometer* in many, routine photometric assays. Using the *flatbed scanner* as a photometer could be very useful in clinics that perform many different analyses on dozens of samples per day. For in-field absorbance measurements on multiple samples, the *camera-based photometer* may prove more suitable due its portability (especially because of the lightness, low power consumption, and mobility of a cell phone compared to a scanner). After using either low-cost photometer to capture images of samples, a user could analyze the images locally (either manually or using a custom software) and/or send them to a central location for remote analysis, interpretation, and logging.

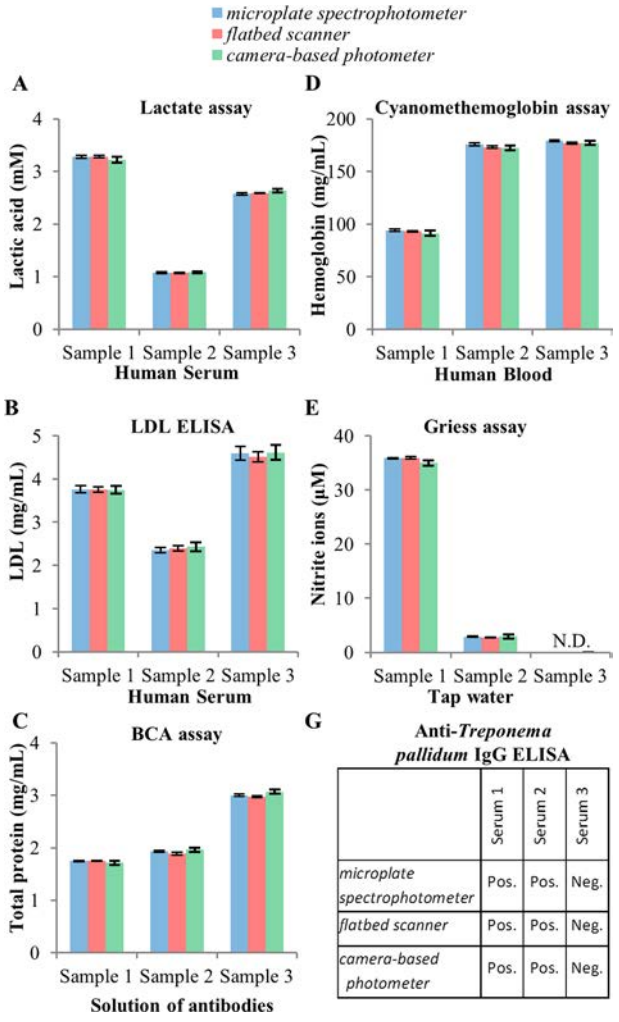


**Figure 5.** Histograms of the results of the analysis of samples using (A) Lactate assay, (B) LDL assay, (C) BCA assay, (D) Cyanomethemoglobin assay, (E) Griess assay, and (G) Anti-*Treponema pallidum* IgG ELISA. All the assays were performed with the *microplate spectrophotometer*, the *flatbed scanner*, and the *camera-based photometer*. The error bars correspond to the standard deviation of seven replicate measurements. Sample concentrations that were lower than the limit of detection were "not determined" (N.D.). Anti-*Treponema pallidum* IgG ELISA provides binary (positive/negative) results.

## CONCLUSIONS

Although devices for digital imaging have been used to measure absorbance in the past, fundamental questions about the quality and the meaning of these optical measurements have not previously been answered. Our optical model, experiments, and analyses yield four conclusions about RGB-based measurements of absorbance. (i) Transmittance-mode imaging is superior to reflectance-mode imaging because the color-uniformity of neighboring pixels in transmittance measurements enables any software for imaging be used for reading the RGB values, and therefore the absorbance, easily and accurately. (ii) The absorbance spectrum of any sample, and therefore, the peak absorbance value collected by narrow-band measurements, is analytically related to the broadband absorbance measured by an RGB-based photometer. (iii) The highest sensitivity measurements are obtained from the RGB color channel that best overlaps with the peak absorbance of the sample. (iv) The accuracy, precision, and linearity of these RGB-based measurements of absorbance are comparable to measurements of the peak absorbance performed by conventional (and expensive) laboratory-based equipment in a wide range of routine photometric assays.

These results show that either a *flatbed scanner* for imaging photographic films, or a *camera-based photometer* (assembled from a planar light source, a cardboard box and a cell-phone camera), can be used as low-cost photometers without major modifications or complex training of operators. Four important characteristics show that these photometers, both based on ubiquitous, low-cost reliable consumer electronic devices, are effective for all common, array-based spectrophotometric assays. (i) They are versatile enough to detect analytes that


DOI: 10.1021/acs.analchem.5b01612
*Anal. Chem.* 2015, 87, 9170−9178

have very different absorption spectra at different wavelengths within the visible spectrum, regardless of the wavelength of the peak absorbance or the shape of the peak. (ii) They are capable of high-throughput measurement of many samples at a time (36−192, depending on the configuration and the device), because every single pixel sensor of the imaging device works as a single detector. Independent photometric measurements can, therefore, be performed simultaneously. (iii) They are affordable and can be easily replaced. (iv) They are portable and lightweight.

There are three potential disadvantages of using the RGB-resolved absorbance in place of the peak absorbance. (i) Measurements of the RGB-resolved absorbance are less sensitive by approximately 1.3−16× (depending on the device and selected color channel) than measurements of narrowband peak absorbance due to the polychromatic nature of RGB-resolved absorbance and nonlinear gamma corrections. (ii) The RGB-based absorbance values of a sample are influenced by the $L(\lambda)$ of the light source and the $S_k(\lambda)$ and $\gamma_k$ of the RGB-based image sensors. Because these parameters differ for different RGB-based photometers, new calibration curves must be acquired when using different equipment. (iii) The low spectral resolution (i.e., broad bandwidth) of RGB channels does not provide sufficient spectral information for unique discrimination between multiple compounds, that absorb in only one and the same color channel, in a mixture, at a time. For example, chlorophyll a exhibits two absorption peaks at 443 and 675 nm and chlorophyll b at 463 and 655 nm (see Figure S-14 in the Supporting Information). In a sample that contains both chlorophyll a and chlorophyll b, therefore, the concentration of chlorophyll b cannot be determined using an RGB-based photometer without further modifications. Adding color filters to the image sensor could improve both the sensitivity and selectivity of measurements by narrowing the bandwidths of the measurements around the absorption peaks of the dyes. The cost of the color filters is low (e.g., less than $50 for a bandpass color filter); therefore, the overall cost of the RGB photometer will remain low. To improve sensitivity and specificity, analytical laboratories could develop and validate low-cost kits specifically tailored for use with RGB-based photometers; that is, they could select or engineer dyes with absorption peaks that coincide best with the RGB channels of common image sensors than those in current test kits. In general, however, the reduced sensitivity of RGB-resolved measurements relative to measurements of the peak absorbance by a laboratory spectrophotometer does not affect the quality (accuracy, precision, and linearity) of the results and, therefore, is not a practical limitation. The inability to identify unknown samples with complex spectra uniquely, or many samples in a mixture, is also not a major limitation because most applications in biochemical and environmental analysis involve the assay of a single dye with a well-known absorbance spectrum that exhibits a single peak.

These simple and affordable alternatives to conventional equipment are suitable for performing precise and accurate measurements of absorbance in resource-limited laboratories. The *camera-based photometer* is particularly well-suited to in field measurements, especially if the cell-phone used is equipped with a software application that can perform all the steps of the data analysis automatically. A range of laboratories that cannot afford to buy a new microplate reader, or repair or replace a broken one, could use scanners for film imaging for research, education, or routine measurements. For example, laboratories that specialize in biochemistry and organic chemistry might use these devices to monitor chemical and biochemical processes. Overall, this approach to low-cost photometry has the potential to reduce the difficulty and cost of common analysis and may facilitate the wider use of such analysis for screening of diseases (e.g., infectious diseases, chronic diseases, malnutrition), comprehensive testing of the quality of food and water (e.g., bacterial contamination, evaluation of authenticity) and enable simple environmental monitoring (e.g., heavy metals, poisonous gases).

## ■ ASSOCIATED CONTENT

### Supporting Information

The Supporting Information is available free of charge on the ACS Publications website at DOI: 10.1021/acs.analchem.5b01612.

Comprehensive description of the experimental procedures and additional data (PDF)

## ■ AUTHOR INFORMATION


### Corresponding Author

*E-mail: gwhitesides@gmwgroup.harvard.edu.


### Author Contributions

The manuscript was written through contributions of all authors. All authors have given approval to the final version of the manuscript.

### Notes

The authors declare no competing financial interest.

## ■ ACKNOWLEDGMENTS

This work was supported by Bill and Melinda Gates Foundation (Award Number 51308) and by a contract from the Defense Threat Reduction Agency (Award Number HDTRA1-14-C-0037).

## ■ REFERENCES


(1) Malkin, R. A. *Annu. Rev. Biomed. Eng.* **2007**, *9*, 567−587.

(2) Martinez, A. W.; Phillips, S. T.; Carrilho, E.; Thomas, S. W.; Sindi, H.; Whitesides, G. M. *Anal. Chem.* **2008**, *80*, 3699−3707.

(3) Cheng, C.-M.; Martinez, A. W.; Gong, J.; Mace, C. R.; Phillips, S. T.; Carrilho, E.; Mirica, K. A.; Whitesides, G. M. *Angew. Chem.* **2010**, *122*, 4881−4884.

(4) Lapresta-Fernández, A.; Capitán-Vallvey, L. F. *Anal. Chim. Acta* **2011**, *706*, 328−337.

(5) Kearns, J.; Tyson, J. *Anal. Methods* **2012**, *4*, 1693−1698.

(6) Hirayama, E.; Sugiyama, T.; Hisamoto, H.; Suzuki, K. *Anal. Chem.* **2000**, *72*, 465−474.

(7) Sharpe, E.; Frasco, T.; Andreescu, D.; Andreescu, S. *Analyst* **2013**, *138*, 249−262.

(8) Lapresta-Fernández, A.; Capitán-Vallvey, L. F. *Sens. Actuators, B* **2008**, *134*, 694−701.

(9) Shen, L.; Hagen, J. A.; Papautsky, I. *Lab Chip* **2012**, *12*, 4240−4243.

(10) Yetisen, A. K.; Martinez-Hurtado, J. L.; Garcia-Melendrez, A.; da Cruz Vasconcellos, F.; Lowe, C. R. *Sens. Actuators, B* **2014**, *196*, 156−160.

(11) Hong, J.; Chang, B.-Y. *Lab Chip* **2014**, *14*, 1725−1732.

(12) Mudanyali, O.; Dimitrov, S.; Sikora, U.; Padmanabhan, S.; Navruz, I.; Ozcan, A. *Lab Chip* **2012**, *12* (15), 2678−2686.

(13) Erenas, M. M.; Cantrell, K.; Ballesta-Claver, J.; de Orbe-Payá, I.; Capitán-Vallvey, L. F. *Sens. Actuators, B* **2012**, *174*, 10−17.

(14) López-Ruiz, N.; Martínez-Olmos, A.; Pérez de Vargas-Sansalvador, I. M.; Fernández-Ramos, M. D.; Carvajal, M. A.;




DOI: 10.1021/acs.analchem.5b01612
*Anal. Chem.* 2015, 87, 9170−9178

Capitan-Vallvey, L. F.; Palma, A. J. *Sens. Actuators, B* **2012**, *171−172*, 938−945.
(15) García, A.; Erenas, M. M.; Marinetto, E. D.; Abad, C. A.; de Orbe-Paya, I.; Palma, A. J.; Capitán-Vallvey, L. F. *Sens. Actuators, B* **2011**, *156*, 350−359.
(16) Preechaburana, P.; Gonzalez, M. C.; Suska, A.; Filippini, D. *Angew. Chem., Int. Ed.* **2012**, *51*, 11585−11588.
(17) Coskun, A. F.; Ozcan, A. *Curr. Opin. Biotechnol.* **2014**, *25*, 8−16.
(18) Göröcs, Z.; Ozcan, A. *Lab Chip* **2014**, *14*, 3248−3257.
(19) Cate, D. M.; Adkins, J. A.; Mettakoonpitak, J.; Henry, C. S. *Anal. Chem.* **2015**, *87*, 19−41.
(20) Ellerbee, A. K.; Phillips, S. T.; Siegel, A. C.; Mirica, K. A.; Martinez, A. W.; Striehl, P.; Jain, N.; Prentiss, M.; Whitesides, G. M. *Anal. Chem.* **2009**, *81*, 8447−8452.
(21) Sia, S. K.; Linder, V.; Parviz, B. A.; Siegel, A.; Whitesides, G. M. *Angew. Chem., Int. Ed.* **2004**, *43* (4), 498−502.
(22) Cohen, A. R.; Seidl-Friedman, J. *Am. J. Clin. Pathol.* **1988**, *90*, 302−305.
(23) Mieczkowska, E.; Koncki, R.; Tymecki, Ł. *Anal. Bioanal. Chem.* **2011**, *399*, 3293−3297.
(24) Duk Han, Y.; Chun, H. J.; Yoon, H. C. *Biosens. Bioelectron.* **2014**, *59*, 259−268.
(25) Albert, D. R.; Todt, M. A.; Davis, H. F. *J. Chem. Educ.* **2012**, *89* (11), 1432−1435.
(26) Quagliano, J. M.; Marks, C. A. *J. Chem. Educ.* **2013**, *90* (10), 1409−1410.
(27) Rohit; Kanwar, L.; Rao, K. K. *Sens. Actuators, B* **2010**, *149*, 245−251.
(28) Sumriddetchkajorn, S.; Chaitavon, K.; Intaravanne, Y. *Sens. Actuators, B* **2014**, *191*, 561−566.
(29) Wei, Q.; Nagi, R.; Sadeghi, K.; Feng, S.; Yan, E.; Ki, S. J.; Caire, R.; Tseng, D.; Ozcan, A. *ACS Nano* **2014**, *8*, 1121−1129.
(30) Medeiros de Morais, C. d. L.; de Lima, K. M. G. *Talanta* **2014**, *126*, 145−150.
(31) Abbaspour, A.; Khajehzadeh, A.; Ghaffarinejad, A. *Analyst* **2009**, *134*, 1692−1698.
(32) Filippini, D.; Svensson, S. P. S.; Lundström, I. *Chem. Commun.* **2003**, *2*, 240−241.
(33) Iqbal, Z.; Filippini, D. *J. Sens.* **2010**, *2010*, 381796.
(34) Tortora, L.; Stefanelli, M.; Mastroianni, M.; Lvova, L.; Di Natale, C.; D'Amico, A.; Filippini, D.; Lundström, I.; Paolesse, R. *Sens. Actuators, B* **2009**, *142*, 457−463.
(35) Alimelli, A.; Filippini, D.; Paolesse, R.; Moretti, S.; Ciolfi, G.; D'Amico, A.; Lundstrom, I.; Di Natale, C. *Anal. Chim. Acta* **2007**, *597*, 103−112.
(36) Filippini, D.; Di Natale, C.; Paolesse, R.; D'Amico, A.; Lundstrom, I. *Sens. Actuators, B* **2007**, *121*, 93−102.
(37) Vashist, S. K.; van Oordt, T.; Schneider, E. M.; Zengerle, R.; Stetten, F.; Luong, J. H. T. *Biosens. Bioelectron.* **2015**, *67*, 248−255.
(38) Hartigan, J. A.; Hartigan, P. M. *Ann. Stat.* **1985**, *13* (1), 70−84.
(39) Cox, D. R.; Hinkley, D. V. *Theoretical Statistics*. Chapman and Hall: London, 1979.
(40) Lukac, R. *J. Real-Time Image Proc.* **2006**, *1*, 45−52.
(41) Nakamura, J. *Image Sensors and Signal Processing for Digital Still Cameras*; Taylor & Francis: Boca Raton, FL, 2006.
(42) Vora, P. L.; Farrell, J. E.; Tietz, J. D.; Brainard, D. H. *IEEE Trans Image Process* **2001**, *10*, 307−316.



DOI: 10.1021/acs.analchem.5b01612
*Anal. Chem.* 2015, 87, 9170−9178